scientific reports

Check for updates

OPEN

A novel hyperbolic tangent-based PID controller tuned by the artificial lemming algorithm for nonlinear steam condenser pressure control

Serdar Ekinci[1], Davut Izci[2,3], Mostafa Jabari[4], Emre Çelik[5], Mohit Bajaj[6,7,8]✉, Pradeep Vishnuram[9] & Olena Rubanenko[10]✉

Precise pressure regulation in nonlinear shell-and-tube steam condensers is essential for maintaining thermal efficiency and operational safety in power generation plants; however, conventional proportional-integral (PI) and proportional-integral-derivative (PID) controllers struggle with nonlinear dynamics, leading to overshoot, slower settling, and reduced robustness. In this regard, a novel hyperbolic tangent-based PID (tanh-PID) controller is developed in this study to introduce smooth nonlinear gain modulation, enabling enhanced damping behavior and improved transient shaping. The recently introduced artificial lemming algorithm (ALA) is employed to optimally tune the proposed controller for integral of time-weighted absolute error minimization. Extensive simulation studies are performed using a comprehensive nonlinear condenser model incorporating steam–air interactions and hot-well dynamics. The proposed strategy is benchmarked against four competitive optimization algorithms (coati optimization algorithm, dandelion optimizer, success-history based adaptive differential evolution with linear population size reduction, and adaptive artificial electric field algorithm) and compared with state-of-the-art PI and fractional-order PID (FOPID) controllers reported in the literature. The ALA-tuned tanh-PID achieves the lowest integral of time-weighted absolute error (2.1189), fastest rise time (0.5960 s), minimal settling time (12.4799 s) and overshoot (5.8056%), along with near-zero steady-state error (4.0776×10^{-4}%), outperforming all compared methods in both transient response and steady-state accuracy. Robustness analyses further confirm superior disturbance rejection and reliable reference tracking under dynamic uncertainties. These results demonstrate that the proposed methodology offers an efficient, low-complexity, and high-performance control solution suitable for real-time deployment in industrial steam condenser systems.

Keywords Steam condenser control, Hyperbolic tangent PID, Artificial lemming algorithm, Nonlinear dynamics, Time-domain performance, Robustness analysis

Shell-and-tube steam condensers play a vital role in thermal power plants by ensuring efficient heat rejection and maintaining the vacuum required for optimal turbine performance. Their behavior, however, is inherently nonlinear and tightly coupled with the dynamic interactions of steam, air, and circulating water. These characteristics make condenser pressure regulation particularly challenging, as even small disturbances in

[1]Department of Computer Engineering, Bitlis Eren University, 13100 Bitlis, Turkey. [2]Department of Electrical and Electronics Engineering, Bursa Uludag University, 16059 Bursa, Turkey. [3]Applied Science Research Center, Applied Science Private University, Amman 11931, Jordan. [4]Department of Astronautics, Electrical and Energy Engineering (DIAEE), "Sapienza" University of Rome, 00185 Rome, Italy. [5]Department of Electrical and Electronics Engineering, Düzce University, Düzce, Turkey. [6]Department of Electrical Engineering, Graphic Era (Deemed to be University), Dehradun 248002, India. [7]Hourani Center for Applied Scientific Research, Al-Ahliyya Amman University, Amman, Jordan. [8]Graphic Era Hill University, Dehradun 248002, India. [9]Department of Electrical and Electronics Engineering, SRM Institute of Science and Technology, Kattankulathur, Chennai 603203, India. [10]Department of Power Plants and System, Vinnytsia National Technical University, Vinnytsia 21000, Ukraine. ✉email: mohitbajajphd@gmail.com; olenarubanenko@vntu.edu.ua

operating conditions can cause performance degradation, reduced power output, and increased operational risk[1,2]. Traditional control schemes often struggle to maintain stable operation in the face of such nonlinearities, motivating the development of more adaptive and robust control solutions.

Proportional–integral (PI) and proportional–integral–derivative (PID) controllers remain widespread in industrial applications due to their simplicity and proven reliability[3–6]. However, their fixed-gain structures limit effectiveness under highly dynamic and uncertain environments, leading to increased overshoot, longer settling durations, and degraded steady-state accuracy during abrupt changes in condenser operating conditions. To overcome these limitations, advanced structures such as two-degree-of-freedom PID[7], fractional-order PID (FOPID) controllers[8–10], cascaded architectures[11–13], and hybrid intelligent controllers integrating fuzzy logic or nonlinear gain updates[14–18] have been proposed. These controllers provide additional tuning flexibility and improved adaptation but introduce significant complexity and require powerful optimization mechanisms to achieve satisfactory results. Recent studies demonstrate that intelligent, bio-inspired, and hybrid optimization techniques have significantly advanced nonlinear control performance. Metaheuristic algorithms have been effectively applied to DC motor and liquid-level systems[19], neural and sliding-mode synchronization in chaotic and multi-agent environments[20,21], and renewable-energy applications through optimized PID and cascaded control structures[22–25]. Further developments in automatic voltage regulation and dynamic stability using refined sinh–cosh, mountain gazelle, and gradient-based optimizers[26–29], along with high-precision aerospace pitch control via sinh–cosh and artificial-rabbits-based designs[30,31], consistently highlight the capability of adaptive and nature-inspired controllers to achieve rapid response, improved damping, and high steady-state accuracy across complex nonlinear systems.

Simultaneously, a large body of research has focused on metaheuristic optimization for controller tuning, utilizing the strengths of nature-inspired search processes to improve transient performance and robustness. Representative contributions include success-history based adaptive differential evolution with linear population size reduction[32], the adaptive artificial electric field algorithm[33], the coati optimization algorithm[34], and the dandelion optimizer[35], which aim to mitigate premature convergence and enhance global search behavior. In condenser-related studies, optimization techniques such as grey wolf optimizer-based PI[36], gazelle optimizer with logarithmic spiral search and greedy selection mechanisms-based PI[37], enhanced version of cooperation search algorithm-based FOPID[38], sinh cosh optimizer-based FOPID[39], and electric eel foraging optimizer-based PI-PDN[40] have demonstrated performance improvements. Model-based predictive approaches have also been applied to shell-and-tube condensers[41,42]. Although these strategies exhibit notable advancements, most remain constrained by high controller complexity, slow optimization convergence, or insufficient disturbance resilience under real-world conditions.

Recent studies have also demonstrated the significance of advanced control techniques and heat transfer enhancement strategies in industrial and domestic thermal systems. Robust adaptive sliding mode controllers have been employed to improve heat exchanger performance in partially metal-foam-filled domains, enabling enhanced heat transfer and outlet temperature regulation under nonlinear operating conditions[43]. Other investigations have analyzed convection heat transfer behavior in porous cavities with differing outlet port locations and complex dynamic heating patterns, revealing the importance of maintaining system stability across fluctuating thermal loads[44]. Solar-integrated heating technologies have also been optimized to reduce electrical energy consumption while improving thermal efficiency through intelligent design and control[45]. These studies further underscore the need for high-performance control solutions capable of handling nonlinear thermal dynamics, supporting the motivation for developing an improved condenser pressure regulation approach.

Addressing this gap, the present study proposes a hyperbolic tangent-based PID (tanh-PID) controller for nonlinear steam condenser pressure regulation. The inclusion of the tanh function introduces a smooth nonlinear gain modulation layer, enabling improved damping and overshoot suppression without sacrificing computational simplicity. To achieve optimal tuning of this nonlinear controller structure, the recently developed artificial lemming algorithm[46] is employed due to its strong exploration–exploitation balance and adaptability for high-dimensional nonlinear optimization. The artificial lemming algorithm's biologically inspired mechanisms (migration, foraging, and predator evasion) allow it to efficiently escape local minima and converge toward high-quality control solutions.

In this study, the proposed artificial lemming algorithm-tuned tanh-PID controller is extensively evaluated through a series of comparative performance analyses. First, the artificial lemming algorithm is benchmarked against four recent and competitive metaheuristic algorithms (coati optimization algorithm[34], dandelion optimizer[35], success-history based adaptive differential evolution with linear population size reduction[32], and adaptive artificial electric field algorithm[33]) to examine optimization effectiveness in minimizing the integral of time-weighted absolute error cost function. Closed-loop time-domain simulations are then conducted to validate reference tracking precision and dynamic stability under nonlinear condenser conditions. Furthermore, the proposed method is compared with several state-of-the-art PI (tuned via gazelle optimizer with logarithmic spiral search and greedy selection mechanisms[37], grey wolf optimizer[36], particle swarm optimization[36] and Ziegler-Nichols[36]) and FOPID (tuned via sinh cosh optimizer[39], whale optimization algorithm[39], enhanced version of cooperation search algorithm[38] and prairie dog optimization[38]) based controllers from the literature, enabling a comprehensive evaluation of transient behavior, steady-state performance, and robustness. The obtained results confirm that the ALA-based tanh-PID controller achieves the lowest integral of time-weighted absolute error value (2.1189), fastest rise time (0.5960 s), and minimal overshoot (5.8056%), while ensuring near-zero steady-state error (4.0776×10^{-4}%). The controller further demonstrates strong resilience against disturbances and parameter variations, validating its practical suitability for nonlinear steam condenser pressure regulation applications. In light of above discussion, the key contributions of this study are summarized as follows:

1. A novel tanh-PID controller is developed to enhance control smoothness, transient shaping, and robustness for nonlinear steam condenser dynamics.
2. The artificial lemming algorithm is utilized for optimal controller tuning, representing its first integration with steam condenser pressure regulation.
3. A complete nonlinear condenser model is used in optimization, incorporating mass, pressure, and energy balance dynamics across steam, air, and hot-well water regions.
4. Extensive simulations are performed using the integral of time-weighted absolute error performance index to quantitatively evaluate control quality.
5. The proposed controller is compared against four modern metaheuristic optimizers and several state-of-the-art PI and FOPID schemes from the literature, demonstrating the lowest integral of time-weighted absolute error (2.1189), fastest rise (0.5960 s), lowest overshoot (5.8056%), and nearly zero steady-state error (4.0776×10^{-4}%).
6. Robustness is validated through reference tracking and disturbance rejection experiments, confirming reliability under dynamic uncertainties.

Overall, this work establishes a new controller optimization framework that successfully combines nonlinear gain shaping with intelligent global optimization for industrial steam condenser applications. The resulting solution maintains computational efficiency and ease of integration which are qualities essential for real-time deployment in modern power generation facilities.

The remainder of the paper is structured as follows: Section "Dynamic modeling of a steam condenser" describes the nonlinear condenser model, Section "Artificial lemming algorithm" outlines the artificial lemming algorithm's optimization mechanism, Section "Proposed novel hyperbolic tangent PID controller" details the proposed tanh-PID controller design, and Section "Nonlinear optimization problem" formulates the optimization problem being considered in this study. Section "Simulation results and discussion" presents comparative simulation results and robustness analyses, while Section "Conclusion" concludes the study and highlights potential future research directions.

Dynamic modeling of a steam condenser

The functioning details of a shell-and-tube steam condenser become clear when you study how steam works with cooling water and the heat exchange surfaces in the system. The common design for this condenser type presents an external form that takes on cylindrical or elliptical shapes which Fig. 1 demonstrates. End closures serve as water chambers and the primary shell contains a perforated tube plate placed between these closures. The tube plate holds several cooling water tubes which are positioned in stacked layers. Steam enters the condenser via an upper inlet pipe connected straight to exhaust equipment or through a compensating component. The bottom tank of the shell captures the condensed liquid while air exits through a lower outlet[1].

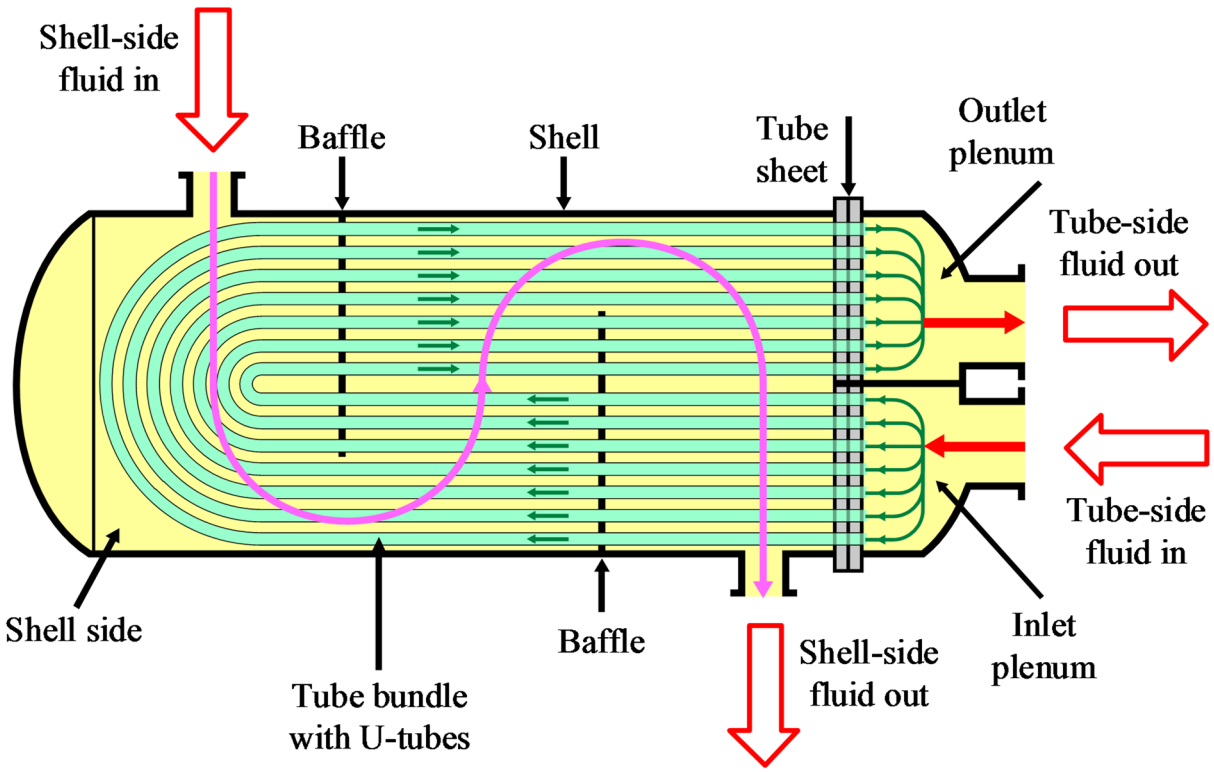


Fig. 1. Conceptual schematic of a steam condenser.

Steam travels through an inlet pipe into the condenser and converts to liquid when it touches the cooler surfaces of the tubes. The condensation process moves heat from the steam into the cooling water circulating inside the tubes. The cooling water enters the condenser at a predetermined temperature and first travels through the bottom set of pipes. The cooling water takes up more heat from the steam as it moves through successive chambers and tubes. The cooling water reaches a higher temperature after passing through several stages before exiting through the outlet pipes to finish the heat exchange cycle.

As the steam and air approach the exhaust section, the ongoing condensation reduces the proportion of steam in the mixture, while the air content gradually rises. The condensation process reaches completion when the air concentration in the entering mixture becomes significant. The mathematical modeling of the condenser's function can be described using governing equations, with those relevant to the steam section detailed in references[1,36,47]. The mathematical expressions governing the steam behavior are formulated as follows:

$$\frac{dG_s}{dt} = G_{st} + G_{ost} - G_c - G_{ss} \tag{1}$$

$$\frac{dP_s}{dt} = \frac{R_s\left(\frac{dG_s}{dt}\right)}{V}(T_s + 273.15) \tag{2}$$

$$\frac{dG_s H_s}{dt} = G_{st} \times H_{st} + G_{ost} \times H_{ost} - (G_c + G_{ss}) \times H_s \tag{3}$$

In these equations, variables such as G_s, G_{st}, G_{ost}, G_c, G_{ss}, P_s, R_s, V, T_s, H_s, H_{st}, and H_{ost} define different parameters, including steam volume within the shell, exhaust steam flow from the turbine, additional steam input, condensed steam output, steam evacuated by vacuum pumps, internal pressure, the steam gas constant, volume of the gas region, saturated gas temperature, and enthalpy values of steam from various sources. Equations (1–3) depict the mass balance of steam, vapor pressure, and the average enthalpy of steam within the condenser. For the air zone, the governing equations are referenced in[1,36,47].

The equations governing air behavior are outlined below:

$$\frac{dG_a}{dt} = G_{vb} + G_n - G_g - G_a \tag{4}$$

$$\frac{dP_a}{dt} = \frac{R_a\left(\frac{dG_a}{dt}\right)}{V}(T_s + 273.15) \tag{5}$$

$$P_C = P_s + P_a \tag{6}$$

Here, the variables G_{vb}, G_n, G_g, G_a, P_a, R_a, and P_C signify the air entering the condenser from the vacuum break valve, air generated by normal drainage condensation, air introduced through seal leaks, air removed by the evacuation system, internal air pressure, the gas constant for air, and the absolute pressure inside the condenser. Equations (4–6) provide a mathematical description of air mass balance, air pressure, and absolute pressure in the condenser. For the heated water region, the governing equations are presented in[1,36,47]. The relevant equations for the hot water section are:

$$L_c = \frac{G_w}{\rho A_w} \tag{7}$$

$$\frac{dG_w}{dt} = G_c + G_{gp} - G_{wo} \tag{8}$$

$$\frac{dG_w H_w}{dt} = G_c \times H_{cw} + G_{gp} \times H_{gp} - (G_{wo} \times H_w) \tag{9}$$

Here, L_c, G_w, ρ, A_w, G_{gp}, G_{wo}, H_{gp}, H_w, and H_{cw} represent the water level in the hot well, quality of hot well water, water density, cross-sectional area of the hot well, volume of expelled oxygen, the outflow of condensed water, enthalpy of exhaust steam carrying oxygen, enthalpy of hot well water, and enthalpy of saturated water at condenser pressure. Equations (7–9) correspond to the hot well water level, water quality, and enthalpy equations. The condenser's tube-side model is derived from the dynamic heat balance equation for circulating water, as discussed in[1,36,47]. The heat balance equation is given by:

$$M_w C_w \frac{dT_2}{dt} = Q - Q_w = UA\Delta t_m - F_{cw} C_p (T - T_{cw}) \tag{10}$$

In this equation, M_w, C_p, Q, Q_w, U, Δt_m, A, F_{cw}, T_{cw}, and T indicate the total circulating water volume, specific heat capacity of water, steam outlet heat, absorbed heat by circulating water, condenser heat transfer coefficient, logarithmic mean temperature difference, heat transfer area, circulating water flow rate, inlet temperature, and outlet temperature of circulating water. The logarithmic mean temperature difference (Δt_m) is determined according to[1,36,47].

$$\Delta t_m = \frac{T - T_{cw}}{\ln\left(\frac{(T_s - T_{cw})}{(T_s - T)}\right)} \tag{11}$$

The calculation of overcooling relies on the difference which equals T_c minus T_w where T_c indicates the saturated water temperature at condenser vapor pressure and T_w refers to the hot well water temperature. The heat transfer discrepancy is determined by calculating δt as the difference between T_s (the saturated gas temperature at the condenser's saturation pressure) and T. When condensation occurs at a constant rate and both entering steam and departing condensate maintain saturation levels, thermal energy transfer equals the steam's latent heat value. The calculation of heat emitted by the steam relies on:

$$\frac{dT}{dt} = \frac{F_{cw}}{M_{cw}}(T_{cw} - T) + \frac{Q}{M_{cw} + C_p} \tag{12}$$

To ensure a stable condensation level under a set vacuum condition, it is necessary to regulate the discharge of condensed water within a specific range. A simplified assumption is that the condensate entering and leaving the system remains saturated. Therefore, the equation describing the ideal gas behavior is given as:

$$\frac{dP}{dt} = \frac{RT_c}{V}(F_s - F_c) \tag{13}$$

The parameters of the steam condenser considered in this study were chosen to be the same as the values reported in[36–39].

Artificial lemming algorithm

The artificial lemming algorithm (ALA) stands as a groundbreaking bio-inspired optimization method which simulates lemming behaviors such as long-distance migration and digging holes while searching for sustenance and avoiding predators. The mathematical models represent these behaviors to maintain a dynamic equilibrium between exploration and exploitation during each phase of optimization. The ALA uses an adaptive energy mechanism to transition its search strategy from broad exploration to detailed exploitation, which improves convergence speed and stability when addressing complex problems with many dimensions. The initialization of ALA is given by:

$$Z_{i,j} = LB_j + rand\,(UB_j - LB_j), \quad i = 1, 2, \ldots, N, \quad j = 1, 2, \ldots..Dim \tag{14}$$

where is a random value in [0,1], LB_j and UB_j represent the lower and upper bounds of the search space. The exploration is modeled as:

$$Z_i(t+1) = Z_{best}(t) + F \times BM \times (R \times (Z_{best}(t) - Z_i(t)) + (1 - R) \times (Z_i(t) - Z_a(t))) \tag{15}$$

where F is a direction flag, BM represents Brownian motion, and R is a random control factor. The exploration is described by:

$$Z_i(t+1) = Z_i(t) + F \times L \times (Z_{best}(t) - Z_b(t)) \tag{16}$$

where, L is a random number influenced by the iteration count. Foraging for food (exploitation) follows a spiral search mechanism:

$$Z_i(t+1) = Z_{best}(t) + F \times spiral \times rand \times Z_i(t) \tag{17}$$

where, spiral is computed as:

$$spiral = radius \times (\sin(2\pi \times rand) + \cos(2\pi \times rand)) \tag{19}$$

In addition, radius is the Euclidean distance between the current position and the best solution. The evading predator's behavior (exploitation) uses Lévy flight:

$$Z_i(t+1) = Z_{best}(t) + F \times G \times Levy(Dim) \times (Z_{best}(t) - Z_i(t)) \tag{19}$$

where, G is an escape coefficient and $Levy(x)$ is defined as:

$$Levy(x) = 0.01 \times \frac{u \times \sigma}{|v|^{\frac{1}{\beta}}}, \quad \sigma = \left(\frac{\Gamma(1+\beta) \times \sin\left(\frac{\pi\beta}{2}\right)}{\Gamma\left(\frac{1+\beta}{2}\right) \times \beta \times 2^{\frac{(\beta-1)}{2}}}\right)^{\frac{1}{\beta}} \tag{20}$$

where, $u, v \sim U(0,1)$ and $\beta = 1.5$. The transition from exploration to exploitation is governed by the energy factor:

$$E(t) = 4 \times arctan\left(1 - \frac{t}{T_{max}}\right) \times \ln\left(\frac{1}{rand}\right) \tag{21}$$

which decreases over iterations to balance the search dynamics. Compared to existing metaheuristic algorithms, ALA effectively avoids premature convergence and maintains diversity in the search space, improving solution accuracy and stability. Its performance is validated through comparisons with state-of-the-art optimization methods on benchmark test suites, demonstrating superior optimization capabilities. The algorithm has also been applied successfully to real-world engineering problems, including constrained design optimization, photovoltaic model parameter identification, and fractional-order PID controller tuning. Figure 2 shows the flowchart of ALA optimization method[46].

Proposed novel hyperbolic tangent PID controller

The conventional PID structure offers simplicity and reliable performance in industrial control; however, its linear gain action often struggles to efficiently handle strong nonlinearities, resulting in overshoot and oscillatory behavior[48]. To enhance transient shaping and steady-state accuracy, a novel hyperbolic tangent-based PID controller (tanh-PID) is designed in this study. The key feature of this structure is the incorporation of a nonlinear gain modulation layer using the hyperbolic tangent function, expressed mathematically as follows.

$$\tanh(x) = \frac{e^{x} - e^{-x}}{e^{x} + e^{-x}} \tag{22}$$

As illustrated in Fig. 3, the function is smooth, continuously differentiable, and bounded within the range $[-1, +1]$. Its gradual slope near the origin provides fine-grain sensitivity for small error values, enabling improved steady-state tracking. Meanwhile, the natural saturation in large-magnitude regions prevents excessively aggressive control actions. This dual behavior introduces an adaptive gain effect that improves damping while limiting overshoot in constraint-sensitive systems such as condenser pressure regulation.

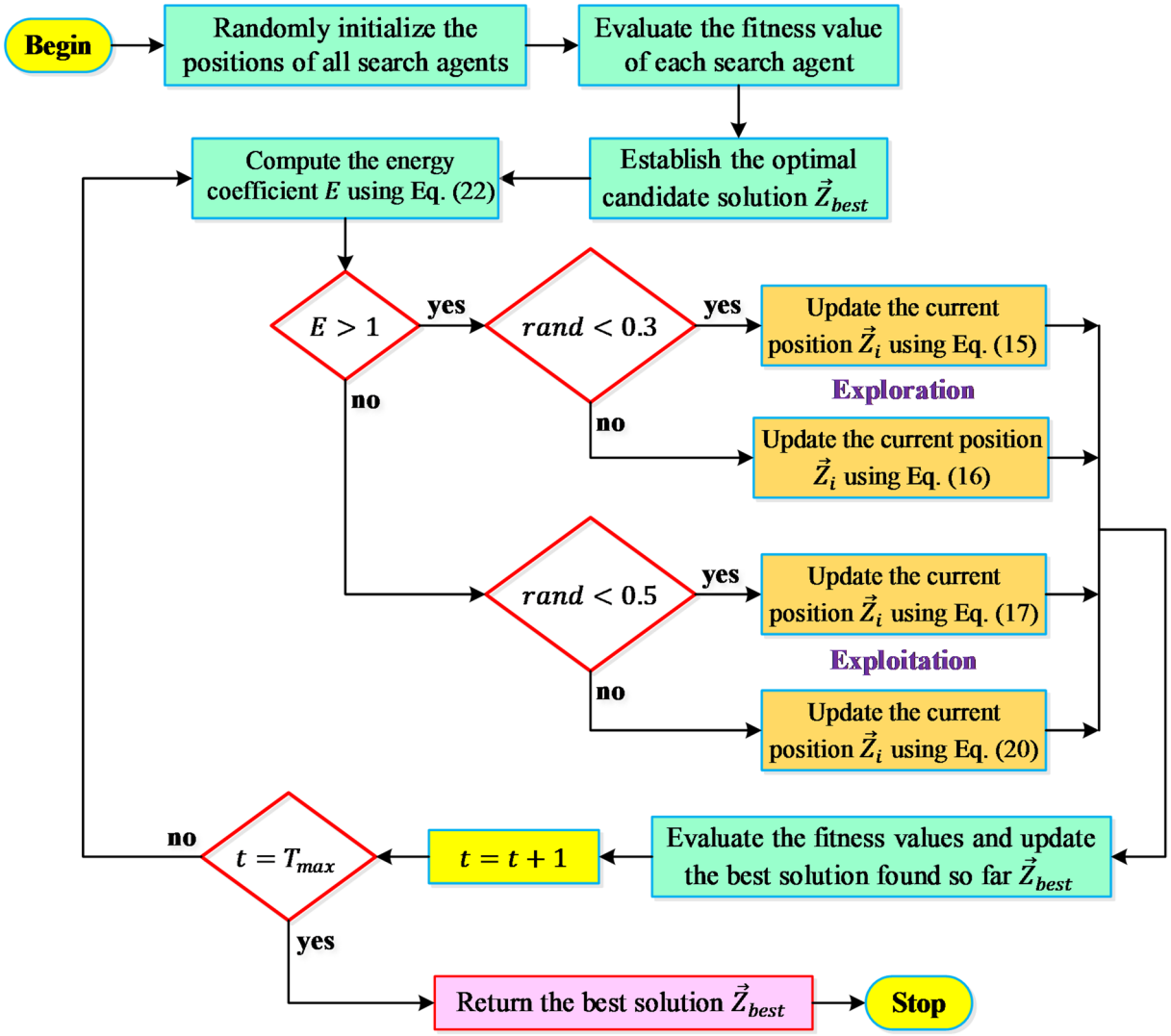


Fig. 2. Flowchart of ALA.

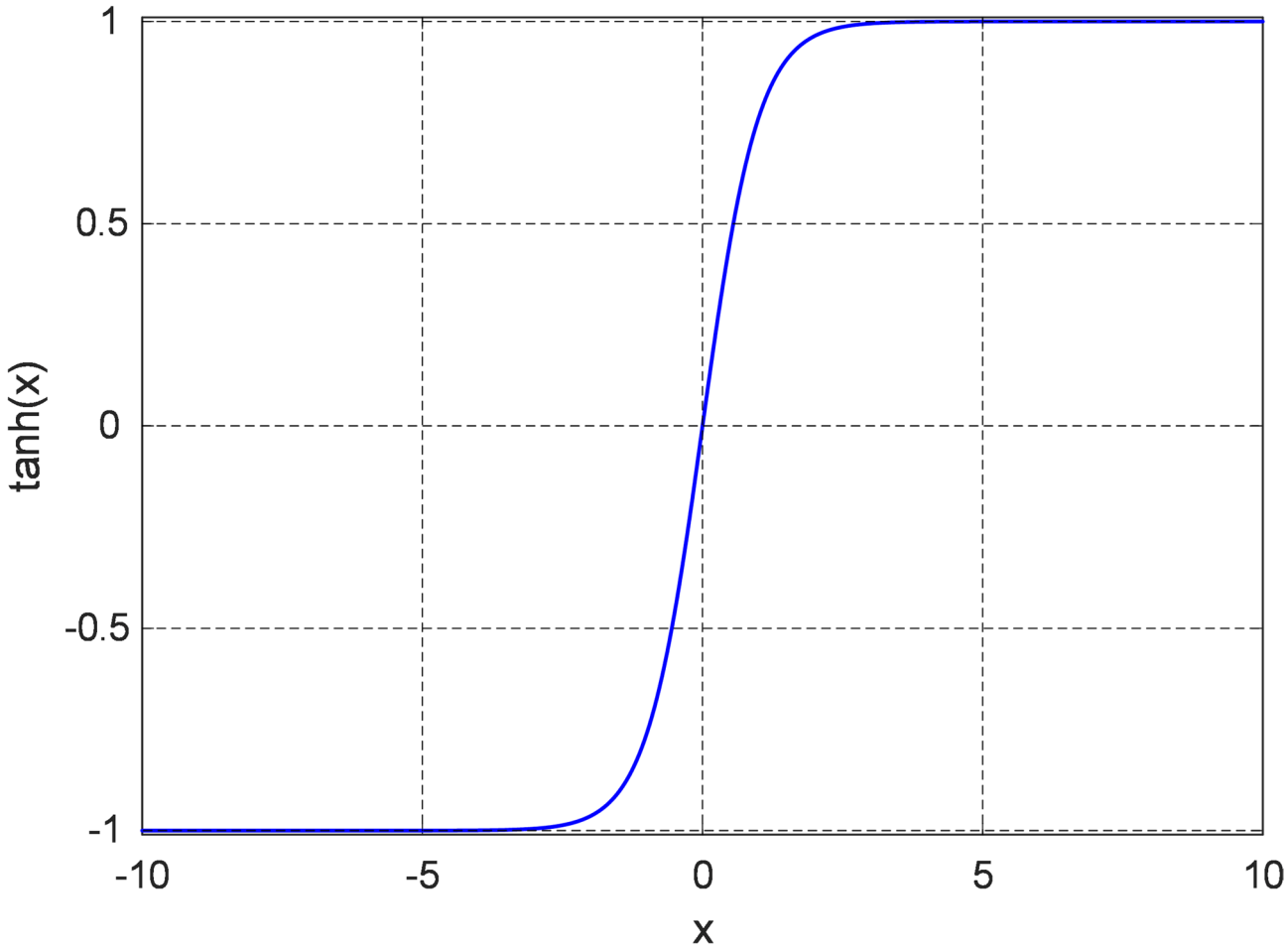


Fig. 3. Plot of hyperbolic tangent function.

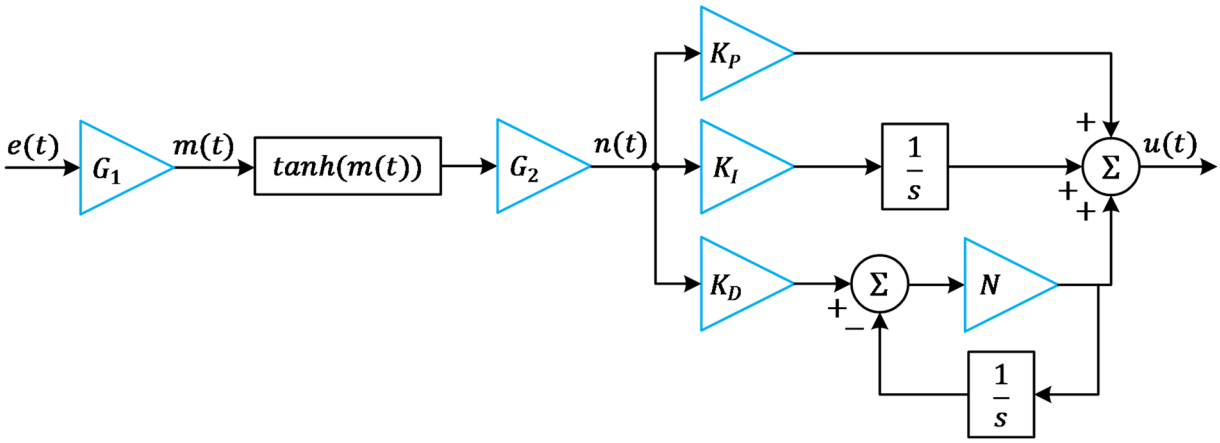


Fig. 4. Block diagram of proposed novel tanh-PID controller.

In the proposed controller, the hyperbolic tangent operator is applied to the combined PID control effort before final actuation. This integration allows the proportional, integral, and derivative terms to contribute in their usual roles while benefiting from nonlinear shaping. The resulting structure modifies controller aggressiveness dynamically according to operating conditions and instantaneous tracking errors. The detailed block configuration of the proposed controller is depicted in Fig. 4.

The regulation begins with the tracking error $e(t)$, which is first amplified through the gain G_1 to produce an intermediate modulating signal $m(t) = G_1 \times e(t)$. This signal is then passed through the nonlinear hyperbolic

tangent function $n(t) = G_2 \times \tanh(m(t))$. As seen, the output of the nonlinear layer, $n(t)$, is subsequently scaled by another adjustable gain G_2 to establish the final control input to the PID core. This two-stage preprocessing enables fine adaptation of the nonlinearity before conventional PID actions are applied. Each component of the PID controller is then driven using the same shaped signal $n(t)$:

- Proportional contribution: $u_P(t) = K_P\, n(t)$
- Integral contribution: $u_I(t) = K_I \int n(t)\, dt$
- Derivative contribution (filtered form): $u_D(t) = K_D(\frac{dn(t)}{dt})\frac{N}{s+N}$ where N acts as the derivative filter coefficient, stabilizing differentiation and reducing noise amplification.

These three contributions are then combined through a summation node to generate the final control output $u(t)$ which equals to $u_P(t) + u_I(t) + u_D(t)$. The filtered-derivative structure enhances robustness and actuator safety by preventing high-frequency spikes, while the nonlinear transformation $n(t)$ ensures smooth bounded control without sacrificing responsiveness. Overall, the tanh-PID architecture modifies the error signal before PID action rather than altering the core gains directly. This strategic placement enables the controller to:

1. Adaptively scale gains during large tracking deviations, preventing overshoot
2. Increase resolution near the zero-error region for superior steady-state precision
3. Improve robustness against disturbances and dynamic steam–air interactions within the condenser

These enhancements make the controller more suitable for nonlinear industrial process environments where standard PID control tends to become aggressive or unstable.

Nonlinear optimization problem

The nonlinear optimization problem in this study is formulated to enhance the performance of the steam condenser system by employing an advanced control methodology. The optimization process is evaluated using the integral of time-weighted absolute error (ITAE) as the cost function, which is defined as[49]:

$$ITAE = \int_{t_1}^{t_2} |e(t)|\,(t - t_1)\, dt \tag{23}$$

where $e(t)$ represents the instantaneous error over time. The ITAE criterion is particularly effective in penalizing sustained errors over longer durations, thereby improving the transient response of the control system. In addition,t_1 and t_2 are 10 s and 50 s respectively.

Table 1 presents the lower and upper bounds for six distinct parameters, essential for achieving optimal control behavior. These parameters span a wide range, indicating the robustness and flexibility of the designed controller. Notably, the proportional and integral gains are constrained between [1, 100] and [0.1, 10], respectively, suggesting a balance between fast response and steady-state accuracy. The derivative gain is limited within [1, 100], highlighting its role in mitigating overshoot while maintaining system stability. Additionally, the parameter controlling the nonlinearity of the tanh function varies between [0.1, 2], ensuring controlled saturation effects. The remaining two parameters, bounded within [5,500] and [0.5, 10], respectively, provide further adaptability to varying system dynamics.

The graphical representation in Fig. 5 illustrates the proposed novel control methodology for the steam condenser system. The schematic encapsulates the integration of the tanh-PID controller within the nonlinear framework, highlighting the functional components and interactions governing the system dynamics. The figure effectively demonstrates how the proposed control strategy modulates the system's response under dynamic conditions, enhancing stability and efficiency. The visual representation further corroborates the necessity of nonlinear control techniques in mitigating fluctuations and ensuring precise regulation of steam pressure and temperature.

Overall, the numerical bounds and graphical depiction substantiate the effectiveness of the proposed methodology. The parameter ranges facilitate a well-tuned control strategy, while the visual analysis underscores the practical application of the controller in a nonlinear setting. The structured optimization process, as reflected in the provided table and Figure, confirms the potential of the tanh-PID approach in improving the operational efficiency of steam condenser systems.

Parameter	Lower bound	Upper bound
K_P	1	100
K_I	0.1	10
K_D	1	100
N	5	500
G_1	0.1	2
G_2	0.5	10

Table 1. Bounds of tanh-PID controller.

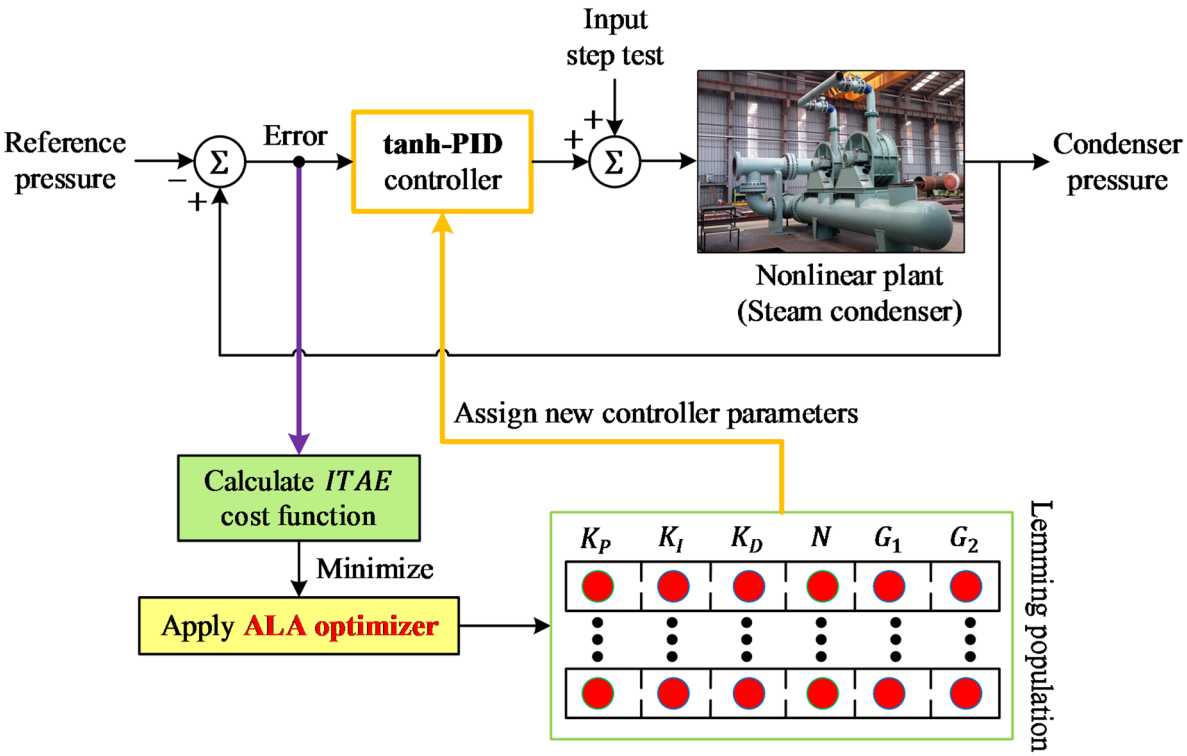


Fig. 5. Illustration of proposed novel control methodology for steam condenser system.

Measure	ALA	COA	DO	L-SHADE	iAEFA
Best	2.1189	3.1392	2.8034	2.2915	2.5087
Worst	2.4030	3.4029	3.2280	2.5704	3.1390
Mean	2.2044	3.2483	2.9396	2.4018	2.6250
SD	0.0678	0.0757	0.0993	0.0673	0.1283

Table 2. Comparison of statistical measurements.

Simulation results and discussion

This section presents a comprehensive performance evaluation of the proposed ALA-tuned tanh-PID controller for nonlinear steam condenser pressure regulation. The optimization algorithms were executed under identical simulation conditions to ensure a fair comparison. Performance assessment was conducted using the ITAE objective function during controller tuning, followed by a closed-loop time-domain evaluation of the optimized parameters. To highlight comparative advantages in terms of convergence behavior and robustness, the ALA is benchmarked against four contemporary metaheuristic techniques: the coati optimization algorithm (COA)[34], dandelion optimizer (DO)[35], success-history based adaptive differential evolution with linear population size reduction (L-SHADE)[32], and adaptive artificial electric field algorithm (iAEFA)[33]. Additionally, the improved tanh-PID controller is compared against several state-of-the-art PI and FOPID configurations reported in the literature to further demonstrate its superiority in dynamic response and tracking accuracy. Numerical results, convergence profiles, and graphical response analyses are presented to validate the effectiveness, reliability, and practical applicability of the proposed control strategy in managing the nonlinear dynamics of steam condenser systems. Each algorithm underwent evaluation through 30 independent runs with a maximum iteration limit T_{max} set to 50 and a population size N of 25.

Statistical analysis of metaheuristic algorithms

A detailed statistical comparison is conducted to assess the optimization performance of the ALA against four contemporary metaheuristic techniques, namely the COA, DO, L-SHADE, and iAEFA. To ensure statistically credible evaluation, each algorithm is executed for 30 independent runs, and four standard performance metrics (best, worst, mean, and standard deviation (SD) of the ITAE objective) are analyzed. The corresponding numerical values are summarized in Table 2.

The results clearly reveal that ALA delivers the most superior solution quality. It achieves the lowest best ITAE value (2.1189) among all competitors, confirming its enhanced global search ability in locating high-performance tanh-PID parameters. Additionally, ALA attains the lowest worst result (2.4030), demonstrating

that even its least favorable optimization trials outperform the comparative algorithms. In contrast, COA produces the highest best (3.1392) and worst (3.4029) results, indicating weaker search behavior and insufficient exploitation. The mean ITAE value emphasizes overall algorithmic effectiveness, where ALA again achieves the smallest value (2.2044), signalling consistent and high-quality convergence over all runs. Conversely, COA yields the largest mean (3.2483), further verifying its inferior reliability in solution refinement. With regard to consistency, ALA and L-SHADE present the lowest dispersion among outcomes, as shown by their SD values of 0.0678 and 0.0673, respectively. This confirms their strong robustness and stability in repeated executions. In comparison, iAEFA exhibits the highest SD (0.1283), reflecting substantial variability and a lower degree of performance predictability. Collectively, this statistical evaluation confirms that ALA offers the best blend of accuracy, reliability, and convergence stability, outperforming both the state-of-the-art algorithms (COA, DO) and advanced evolutionary optimizers (L-SHADE, iAEFA). Accordingly, ALA emerges as the most effective optimization strategy for tanh-PID controller tuning in nonlinear steam condenser pressure regulation.

Evolution of cost function and optimal tanh-PID controller parameters

The convergence behavior of the optimization algorithms is examined through the cost function evolution curves plotted in Fig. 6, where the ITAE objective function is tracked over 50 iterations with a population size of 25. As illustrated, the ALA achieves a faster and smoother reduction in the ITAE value compared to the COA, DO, L-SHADE, and the iAEFA. While COA and DO display a slower descent with noticeable oscillations, L-SHADE and iAEFA demonstrate comparatively better convergence stability. However, their final cost values remain higher than that of ALA, confirming its superior ability to balance exploration and exploitation throughout the search process.

Table 3 reports the optimal tanh-PID controller parameters achieved by each algorithm following convergence. Six parameters are optimized, where the first three correspond to the proportional, integral, and derivative gain components of the control structure. The fourth parameter influences nonlinear gain modulation through the hyperbolic tangent function, while the remaining two parameters contribute to transient shaping and damping characteristics in the controller response. The numerical results reveal clear distinctions among the tested algorithms. The trends in Table 3 show that ALA identifies a well-balanced combination of controller gains and nonlinear shaping parameters, which directly contributes to its superior transient and steady-state

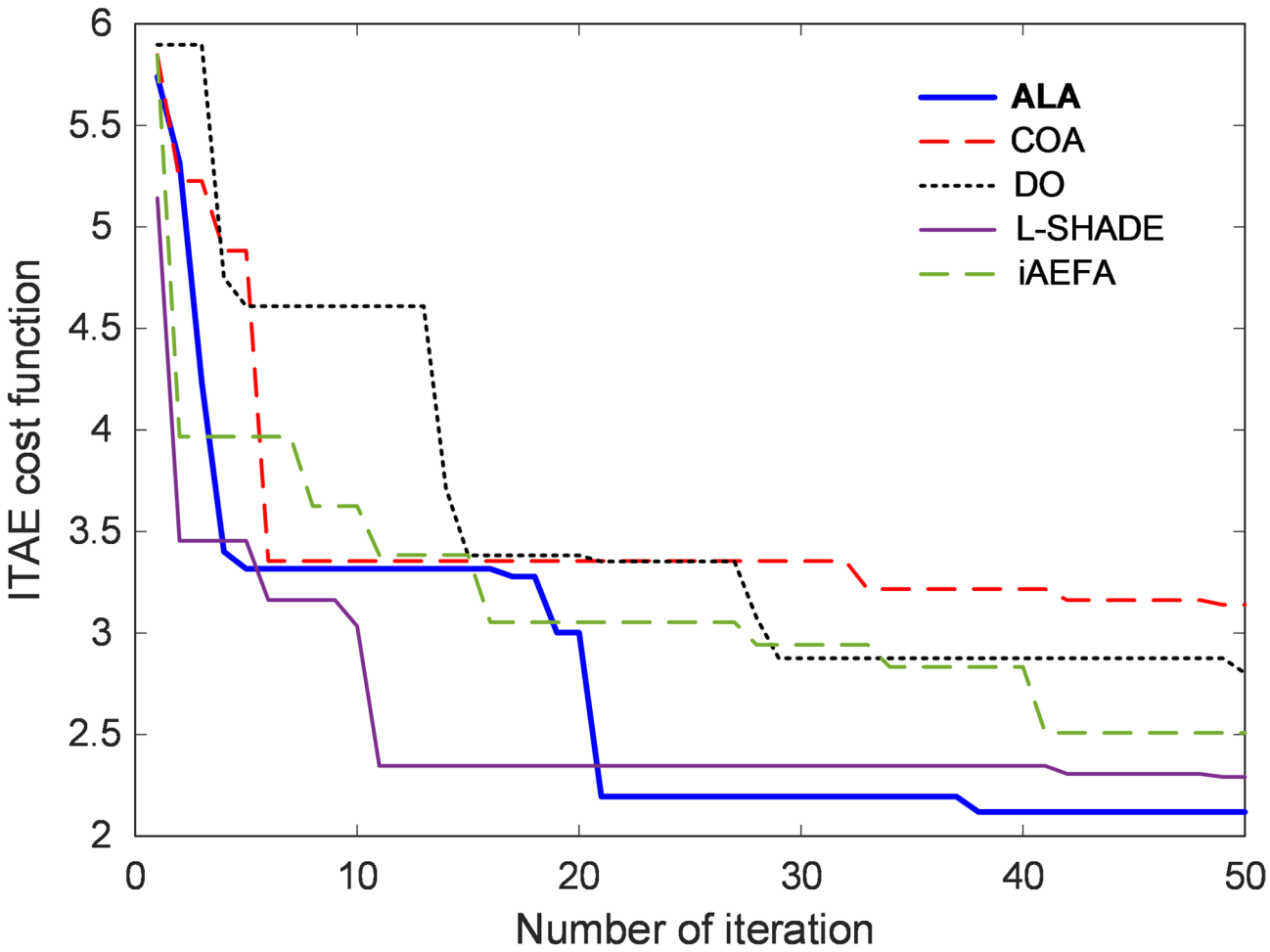


Fig. 6. Change of $ITAE$ cost function.

Parameter	ALA	COA	DO	L-SHADE	iAEFA
K_P	62.8099	46.8660	36.9210	99.4851	30.61920
K_I	0.9346	4.1925	1.3711	1.4760	2.4310
K_D	64.4927	40.8494	59.2916	69.5062	33.8680
N	351.6696	68.3416	108.5362	422.1398	157.1345
G_1	0.3364	0.5293	0.4695	0.2455	0.5250
G_2	7.6861	1.7980	4.3482	5.9515	3.1702

Table 3. Optimal tanh-PID controller parameters.

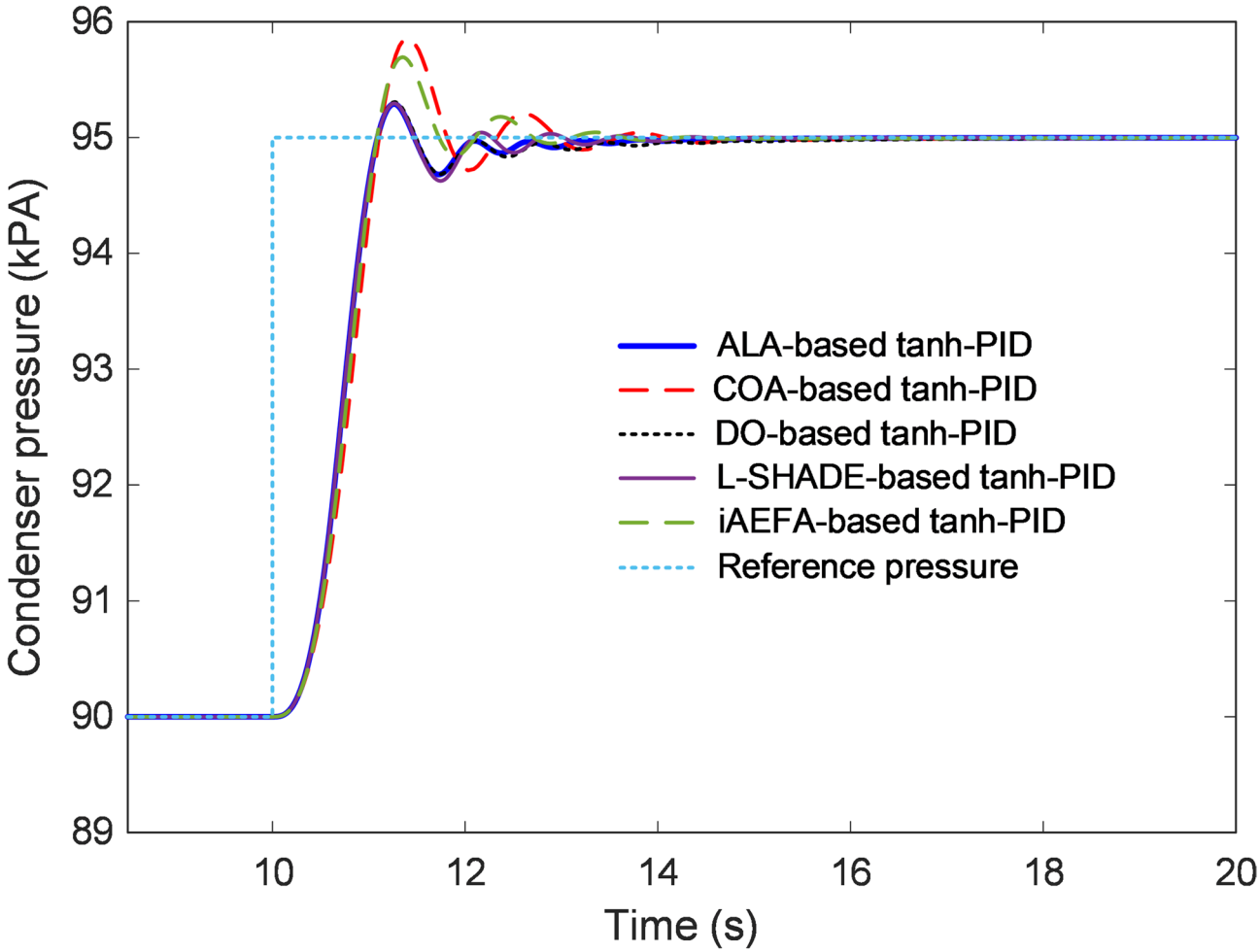


Fig. 7. Output response curves of condenser pressure for tanh-PID controlled system.

performance observed in the later subsections. In contrast, the competing algorithms either emphasize overly aggressive gains (e.g., L-SHADE) or produce conservative settings (e.g., COA), explaining the performance deficiencies seen in their pressure response characteristics.

Closed-loop response

The closed-loop pressure responses of the tanh-PID controlled condenser system optimized by each metaheuristic algorithm are presented in Fig. 7, with the transient behaviors illustrated in detail in Fig. 8. These simulations validate how the optimized controller parameters in Table 3 influence system dynamics once deployed in actual control action. As previously noted, the ALA obtains a well-balanced parameter set, and this distinction becomes evident in the time-domain responses.

Quantitative evaluation of the transient characteristics is summarized in Table 4, where five key indicators (normalized rise time, normalized settling time, normalized overshoot, normalized peak time, and normalized steady-state error) are reported alongside the corresponding ITAE performance measure. The ALA-tuned tanh-

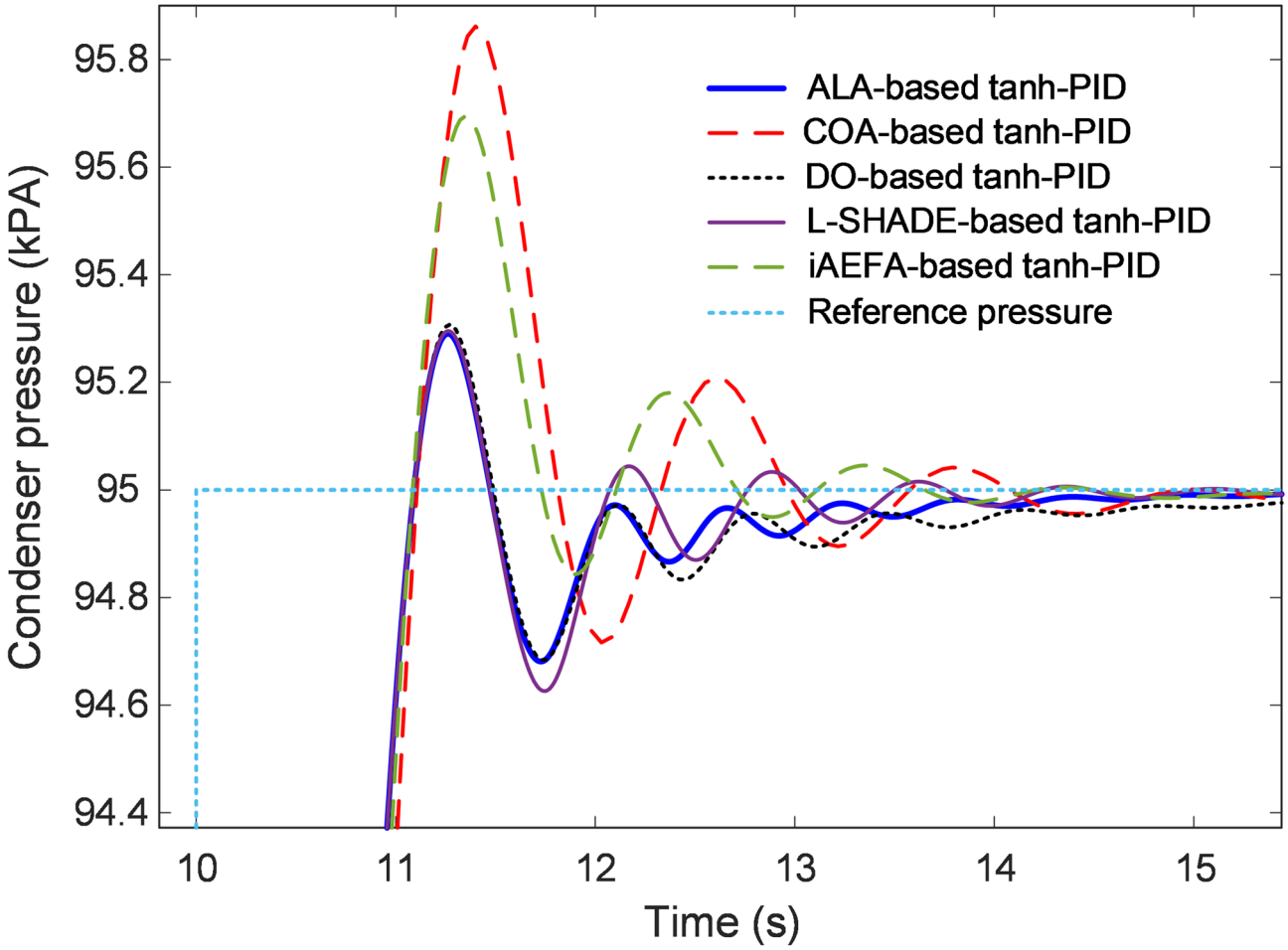


Fig. 8. Comprehensive illustration of transient response in Fig. 7

Performance indicator	ALA	COA	DO	L-SHADE	iAEFA
Normalized rise time (s)	0.5960	0.6260	0.5991	0.5962	0.6052
Normalized settling time (s)	12.4799	13.2795	13.1684	12.6048	12.5586
Normalized overshoot (%)	5.8056	17.2375	6.1521	5.9038	13.9045
Normalized peak time (s)	11.2620	11.4002	11.2729	11.2630	11.3499
Normalized steady-state error (%)	4.0776E−04	0.0012	0.0015	0.0082	6.2331E−04
ITAE cost function	2.1189	3.1392	2.8034	2.2915	2.5087

Table 4. Comparison of performance indicators for tanh-PID controlled system.

PID controller exhibits the fastest normalized rise time of 0.5960 s, enabling rapid pressure elevation toward the reference without initial delay. The rise times of COA (0.6260 s) and DO (0.5991 s) remain slightly slower, while iAEFA (0.6052 s) trails behind. L-SHADE achieves a similar rise time (0.5962 s), but its other performance metrics reveal weaknesses in response refinement.

Similarly, ALA delivers the shortest normalized settling time of 12.4799 s, indicating an earlier transition into steady-state operation. All competitors require longer durations to stabilize (particularly COA (13.2795 s) and DO (13.1684 s)) suggesting weaker damping properties compared with ALA. The settling times of L-SHADE (12.6048 s) and iAEFA (12.5586 s) remain close but still inferior to the ALA-based design.

The overshoot performance further highlights the advantages of the proposed approach. ALA maintains a low and controlled overshoot of 5.8056%, preventing excessive pressure excursions above the desired setpoint. In contrast, COA yields the highest overshoot of 17.2375%, while iAEFA also produces a significant overshoot (13.9045%); both indicative of aggressive or poorly damped control behavior. DO and L-SHADE perform moderately (6.1521% and 5.9038%, respectively), though still not surpassing ALA.

All controllers achieve near-identical normalized peak times around 11.27 s, yet ALA secures the smallest value (11.2620 s), reflecting finely tuned tracking behavior. Meanwhile, the normalized steady-state error results

show ALA achieving the lowest tracking inaccuracy of 4.0776×10^{-4}%, effectively eliminating long-term deviation from the desired condenser pressure. Other methods exhibit larger residual errors, with L-SHADE demonstrating the weakest performance (0.0082%), which aligns with its relatively uneven parameter distribution seen earlier. Finally, the ITAE cost function values in Table 4 reinforce the cumulative performance advantage of ALA. Its value (2.1189) is the lowest across all tested algorithms, confirming a better balance between prompt transients and minimized long-duration error penalties. Although L-SHADE (2.2915) and DO (2.8034) yield competitive results, neither achieves the same consistency and control precision.

Comparative analysis of proposed method and reported PI control approaches

To further verify the performance advantages of the proposed control framework, the ALA-based tanh-PID controller is compared against multiple PI-based control strategies reported in recent literature, namely the gazelle optimizer with logarithmic spiral search and greedy selection mechanisms (Ls-GOA)-based PI[37], grey wolf optimizer (GWO)-based PI[36], particle swarm optimization (PSO)-based PI[36] and Ziegler-Nichols (ZN)-based PI[36] methods. The condenser pressure responses corresponding to these controllers are illustrated in Fig. 9, while the associated quantitative performance indices are summarized in Table 5.

As indicated, the proposed controller significantly enhances the transient response characteristics compared with all PI-based benchmarks. The normalized rise time for the ALA-based tanh-PID is 0.5960 s, which is markedly faster than the competing techniques. The PI controllers tuned using Ls-GOA, GWO, and PSO yield considerably larger rise times (2.0267 s, 1.4436 s, and 1.0513 s, respectively) while the ZN-based PI shows a slightly improved transient (0.7349 s) but still falls short of the proposed approach. The noticeably slower rise in these methods indicates less effective transient shaping during initial pressure elevation.

Regarding normalized settling time, the superiority of the proposed controller is even more prominent. The ALA-based tanh-PID stabilizes within 12.4799 s, achieving the earliest convergence among all compared controllers. In contrast, Ls-GOA-based PI (18.9174 s) and GWO-based PI (19.8228 s) demonstrate substantially prolonged stabilization, while PSO-based PI (24.9424 s) and ZN-based PI (112.0390 s) present significantly sluggish responses. The extended settling durations in these controllers are reflected visually in Fig. 9, where noticeable oscillations persist before reaching steady-state conditions.

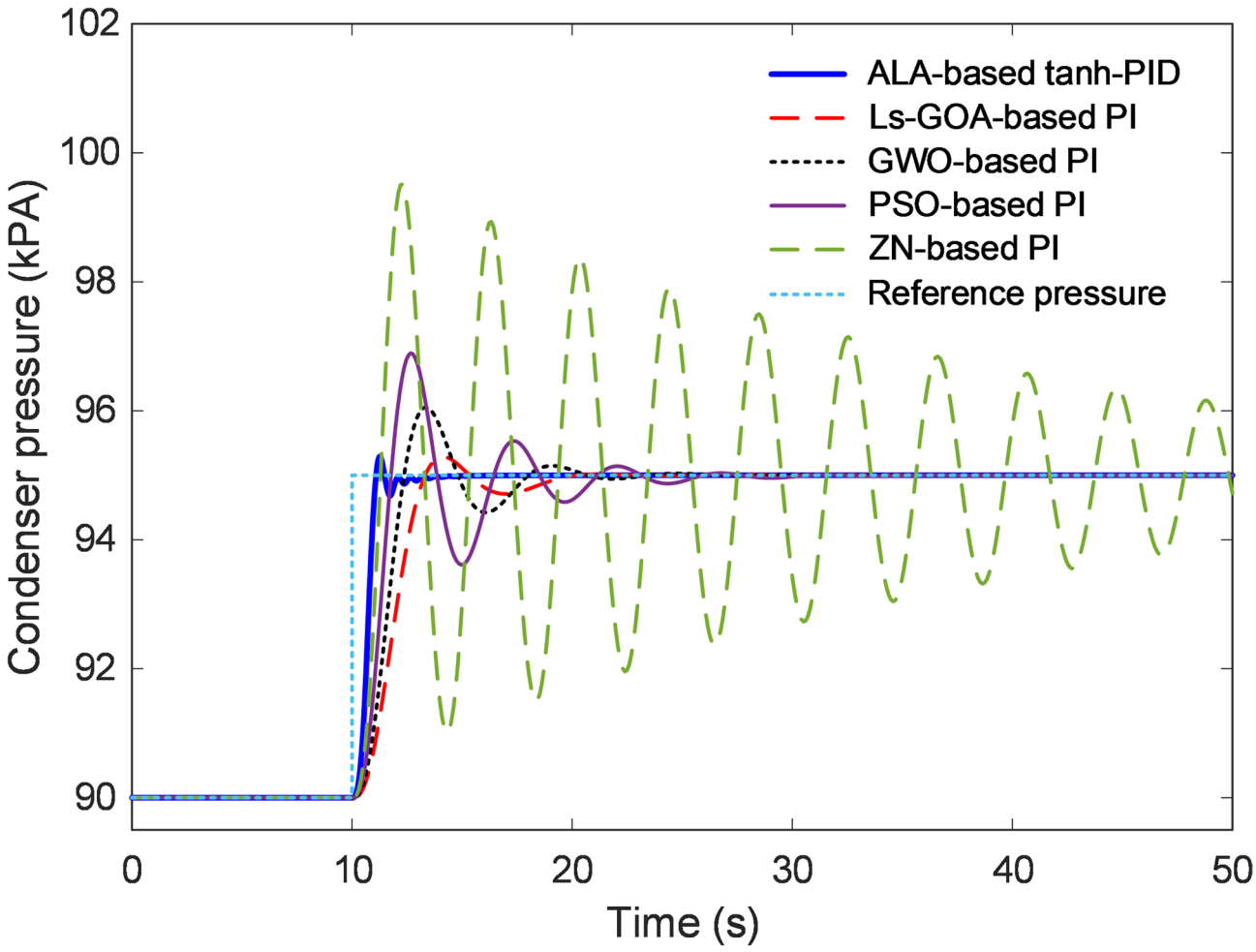


Fig. 9. Output response curves of condenser pressure for ALA-based tanh-PID and other reported PI controlled systems.

Performance indicator	ALA-based tanh-PID	Ls-GOA-based PI	GWO-based PI	PSO-based PI	ZN-based PI
Normalized rise time (s)	0.5960	2.0267	1.4436	1.0513	0.7349
Normalized settling time (s)	12.4799	18.9174	19.8228	24.9424	112.0390
Normalized overshoot (%)	5.8056	5.7279	21.0680	37.8753	90.2549
Normalized peak time (s)	11.2620	14.1223	13.3639	12.6667	12.2966
Normalized steady-state error (%)	4.0776E−04	0.0041	0.0021	0.0112	5.6251
ITAE cost function	2.1189	19.1952	23.8138	43.0814	985.3519

Table 5. Comparison of performance indicators for ALA-based tanh-PID and other reported PI controlled systems.

The overshoot behavior further reveals the advantages of the nonlinear design. While the ALA-based tanh-PID maintains overshoot at a controlled level of 5.8056%, the GWO-based and PSO-based PI controllers exhibit aggressive peak excursions (21.0680% and 37.8753%, respectively), suggesting weaker damping injection in their control actions. The ZN-based PI controller produces an extremely high overshoot (90.2549%), which poses considerable risk in safety–critical condenser pressure regulation. Only the Ls-GOA-based PI shows a slightly lower overshoot than the proposed method (5.7279%), though this comes at the expense of longer rise and settling times. The normalized peak time trends additionally support the superiority of the nonlinear controller, with the proposed approach achieving a minimum of 11.2620 s, whereas the others require 12.2966–14.1223 s, confirming slower and less accurate peak response alignment.

The steady-state accuracy is one of the clearest differentiators. The ALA-tuned tanh-PID attains a negligible tracking error of 4.0776×10^{-4}%, demonstrating precise reference regulation. The other PI structures display significantly larger residual errors, especially the ZN-based PI which suffers from 5.6251% steady-state deviation (three to four orders of magnitude higher than the proposed method).

Finally, the ITAE performance index, which simultaneously reflects transient quality and error suppression, confirms the clear improvement achieved by the proposed controller. The lowest ITAE value of 2.1189 belongs to the ALA-based tanh-PID, whereas the literature-based PI controllers yield far higher values, such as 19.1952 (Ls-GOA-PI), 23.8138 (GWO-PI), and 43.0814 (PSO-PI). The ZN-based PI results in an excessively large ITAE of 985.3519, reinforcing its inadequacy for this nonlinear system.

Comparative analysis of proposed method and reported FOPID control approaches

To further validate the control effectiveness of the proposed ALA-based tanh-PID controller, additional benchmark comparisons were conducted against advanced fractional-order PID (FOPID) controllers previously developed for nonlinear steam condenser pressure regulation. The considered methods include the sinh cosh optimizer (SCHO)-based FOPID[39], whale optimization algorithm (WOA)-based FOPID[39], enhanced version of cooperation search algorithm (en-CSA)-based FOPID[38] and prairie dog optimization (PDO)-based FOPID[38]. Their corresponding condenser pressure responses and transient behaviors are illustrated in Fig. 10, while the quantified performance indicators are provided in Table 6.

As observed from Fig. 10, the proposed controller yields the most rapid tracking and damping behavior, transitioning swiftly toward the reference trajectory with minimal oscillatory deviation. The normalized rise time is substantially improved, where the ALA-based tanh-PID achieves 0.5960 s, markedly lower than those obtained using the SCHO-based (1.7037 s) and WOA-based (1.6415 s) FOPID controllers. Even the most competitive FOPID alternative, the PDO-based design (1.2037s), requires more than twice the rise duration compared with the proposed approach. This improvement indicates an enhanced transient shaping capability driven by the embedded nonlinear gain regulation.

Superior stabilization characteristics are also evidenced in the settling performance. The ALA-tuned tanh-PID enters steady-state ($\pm 2\%$ tolerance band) after 12.4799 s, offering earlier convergence relative to all FOPID counterparts, particularly PDO-based FOPID, which stabilizes only after 18.5321 s. These results demonstrate the proposed controller's stronger damping action and reduced susceptibility to slow decay in the condenser's pressure response.

Overshoot behavior reinforces these observations. The proposed controller achieves a contained overshoot of 5.8056%, whereas the WOA-based and PDO-based FOPID controllers exhibit considerably higher peak excursions (8.1506% and 19.2106%, respectively). Although the SCHO-based structure yields a moderately close value (6.0647%), this minor benefit is offset by its slower response and delayed stabilization. Peak-time characteristics reflect similar trends, with the proposed controller achieving the earliest peak (11.2620 s) among all compared methods. The remaining techniques exhibit slower peak behavior, confirming less precise synchronization with the reference during rapid transient conditions. The normalized steady-state error is another distinctive advantage of the proposed method.

The ALA-tuned tanh-PID maintains a nearly zero tracking error (4.0776×10^{-4}%), which is markedly smaller than those of all FOPID benchmarks, especially the PDO-based FOPID that suffers from a residual deviation of 0.0924%. Finally, the ITAE index, a holistic indicator of long-duration transient quality, demonstrates a significant improvement. The proposed controller achieves the lowest ITAE value of 2.1189, while the en-CSA-based FOPID remains the closest competitor (12.3398) yet still an order of magnitude inferior. The other methods yield substantially higher values, indicating persistent long-term error components and less efficient energy dissipation during transient evolution.

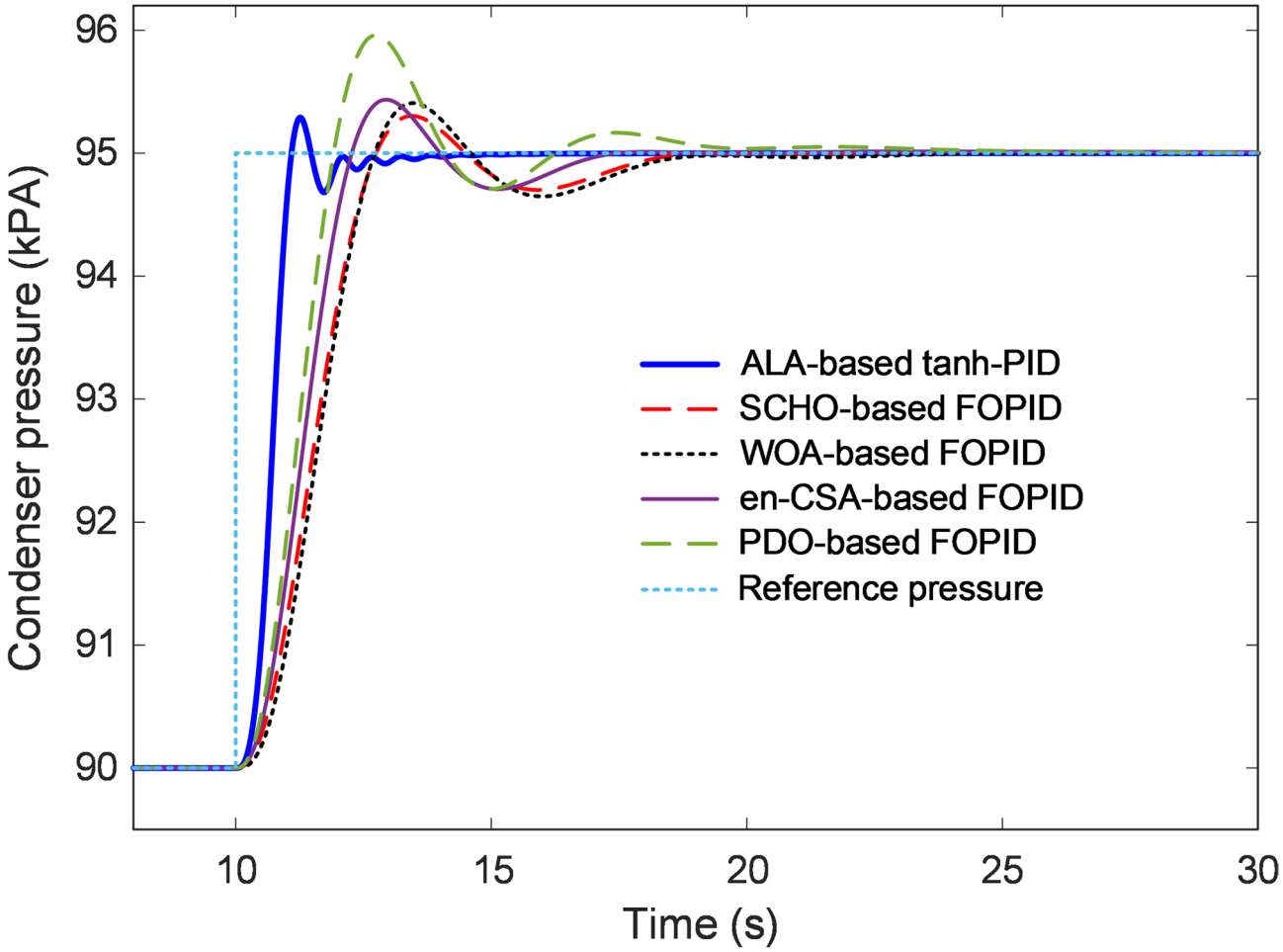


Fig. 10. Output response curves of condenser pressure for ALA-based tanh-PID and other reported FOPID controlled systems.

Performance indicator	ALA-based tanh-PID	SCHO-based FOPID	WOA-based FOPID	En-CSA-based FOPID	PDO-based FOPID
Normalized rise time (s)	0.5960	1.7037	1.6415	1.4095	1.2037
Normalized settling time (s)	12.4799	17.6635	17.9283	16.5104	18.5321
Normalized overshoot (%)	5.8056	6.0647	8.1506	8.7070	19.2106
Normalized peak time (s)	11.2620	13.4467	13.4683	12.9427	12.7455
Normalized steady-state error (%)	4.0776E−04	0.0064	0.0652	0.0090	0.0924
ITAE cost function	2.1189	14.8083	18.2820	12.3398	17.9525

Table 6. Comparison of performance indicators for ALA-based tanh-PID and other reported FOPID controlled systems.

Assessment of robustness characteristics of proposed ALA-based tanh-PID control strategy

The performance of the proposed ALA-based tanh-PID control strategy is assessed by its tracking accuracy for reference pressure and its effectiveness in handling external disturbances and rejecting perturbations. Figures 11, 12, 13 demonstrate the controller performance under various operating conditions. Figure 11 illustrates how the ALA-based tanh-PID controller manages reference pressure tracking. The system performance tracks the reference trajectory with minimal deviation throughout the operation time. The controller maintains system stability because its smooth stable tracking behavior shows effective reduction of steady-state errors. The small observed differences result from built-in system nonlinearities and unpredictable external factors. The controller shows fast alignment with the targeted reference point proving its capability to accurately respond to pressure demand changes.

Figure 12 shows the system's external disturbances variations over time. These disturbances indicate possible operational condition changes including load variations along with environmental factors and unmodeled

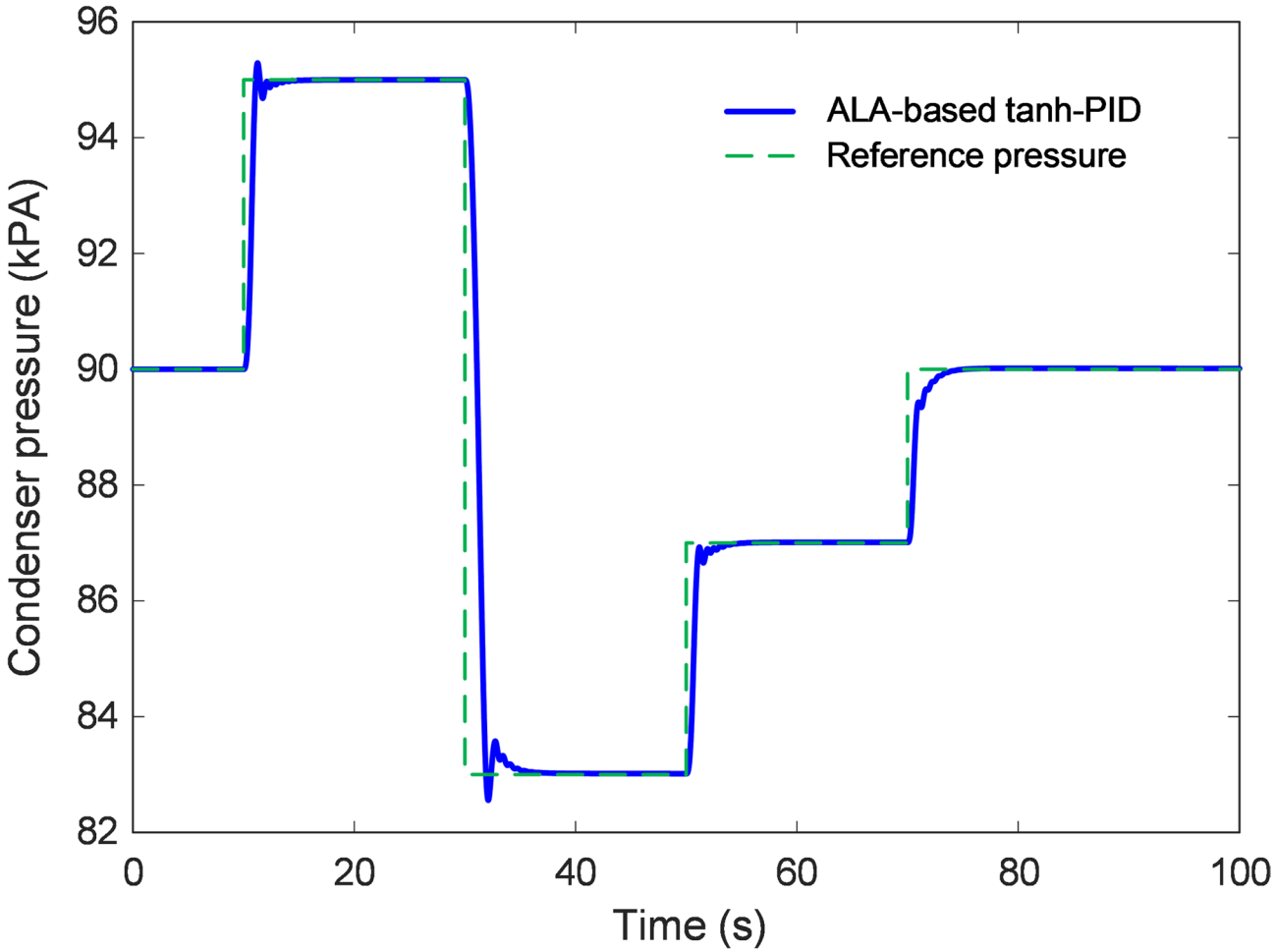


Fig. 11. Reference pressure tracking capability of ALA-based tanh-PID controller.

dynamics. This figure demonstrates how the disturbances develop over time to test the controller's robustness against real-world perturbations.

Figure 13 demonstrates how well the proposed control strategy can reject external disturbances. When disturbances are introduced to the system the controller quickly responds with compensation actions to minimize their impact on system operations. The system's transient response is well-damped and shows minimal overshoot while achieving a swift return to nominal operating conditions. The controller's response demonstrates how the ALA-based tanh-PID system effectively maintains stability while providing resilience to external disturbances. The control approach's ability to dynamically adjust to different disturbances becomes evident through smooth trajectory restoration which confirms its robustness for practical applications needing reliable control solutions.

The examination of Figs. 11, 12, 13 validates the advanced robustness features of the proposed ALA-based tanh-PID control system. The combination of precise reference pressure tracking, disturbance response, and perturbation rejection demonstrates this system's effectiveness in managing complex control situations. The results demonstrate that the proposed approach shows promise for use in applications where high precision and disturbance resilience is essential.

Conclusion

This study presented a novel hyperbolic tangent-based PID controller optimized using the ALA for nonlinear steam condenser pressure regulation. The hyperbolic tangent function was employed to introduce a smooth nonlinear gain adaptation, enhancing overshoot suppression and steady-state accuracy without increasing structural complexity. The controller parameters were optimized by minimizing the ITAE criterion within a comprehensive nonlinear condenser model incorporating steam, air, and hot-well dynamics. Extensive comparative evaluations were conducted to validate the proposed approach. First, ALA was benchmarked against four competitive and recently developed metaheuristic optimizers (COA, DO, L-SHADE, and iAEFA). ALA achieved the lowest best ITAE value of 2.1189, the lowest mean of 2.2044, and a low standard deviation of 0.0678, highlighting both its accuracy and consistency in identifying optimal controller gains. When deployed in closed-loop control, the ALA-tuned tanh-PID demonstrated the fastest rise time (0.5960 s), shortest settling time (12.4799 s), smallest overshoot (5.8056%), earliest peak (11.2620 s), and nearly zero steady-state error

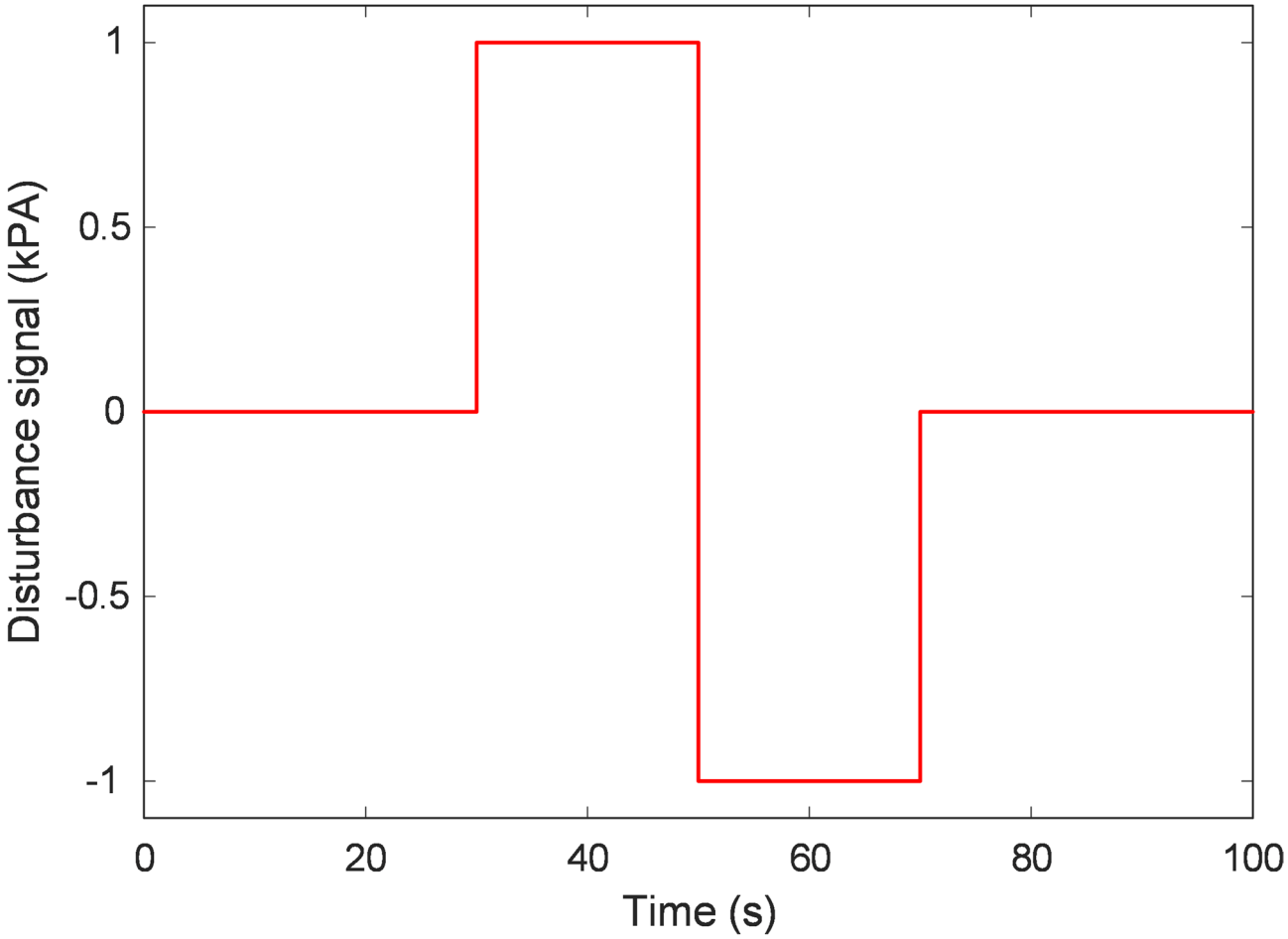


Fig. 12. Change of external disturbance.

(4.0776×10^{-4}%) among all compared optimizers. Additional benchmarking against recently reported PI- and FOPID-based controllers from the literature further validated the dynamic performance improvements of the proposed approach. For instance, while competing PI controllers exhibited overshoots as high as 90.2549% and ITAE values up to 985.3519, the proposed controller retained a compact overshoot of 5.8056% and a minimal ITAE of 2.1189. Similarly, relative to advanced FOPID designs, the proposed strategy delivered up to 2.9 × faster rise time, significantly reduced settling behavior, and up to one order of magnitude improvement in ITAE performance. Robustness assessments demonstrated strong disturbance rejection and reliable tracking capability under dynamic uncertainties, confirming that the nonlinear shaping integrated within the controller structure enhances resilience to real-world operational variations. Overall, the results establish that combining nonlinear gain modulation with an intelligent ALA-based optimization mechanism yields a high-performance control solution suitable for practical deployment in industrial steam condenser systems.

Future works may potentially focus on extending the presented approach toward experimental validation through hardware-in-the-loop or pilot-scale implementations. Stability-theoretic assessments and adaptive versions of the nonlinear control structure may also be explored to support real-time operation under broader uncertainty conditions and evolving condenser performance characteristics. In addition, further research may evaluate multi-objective optimization to jointly address disturbance rejection, control energy efficiency, and actuator health. Updates to the relevant references reflecting these emerging directions have also been incorporated into the manuscript.

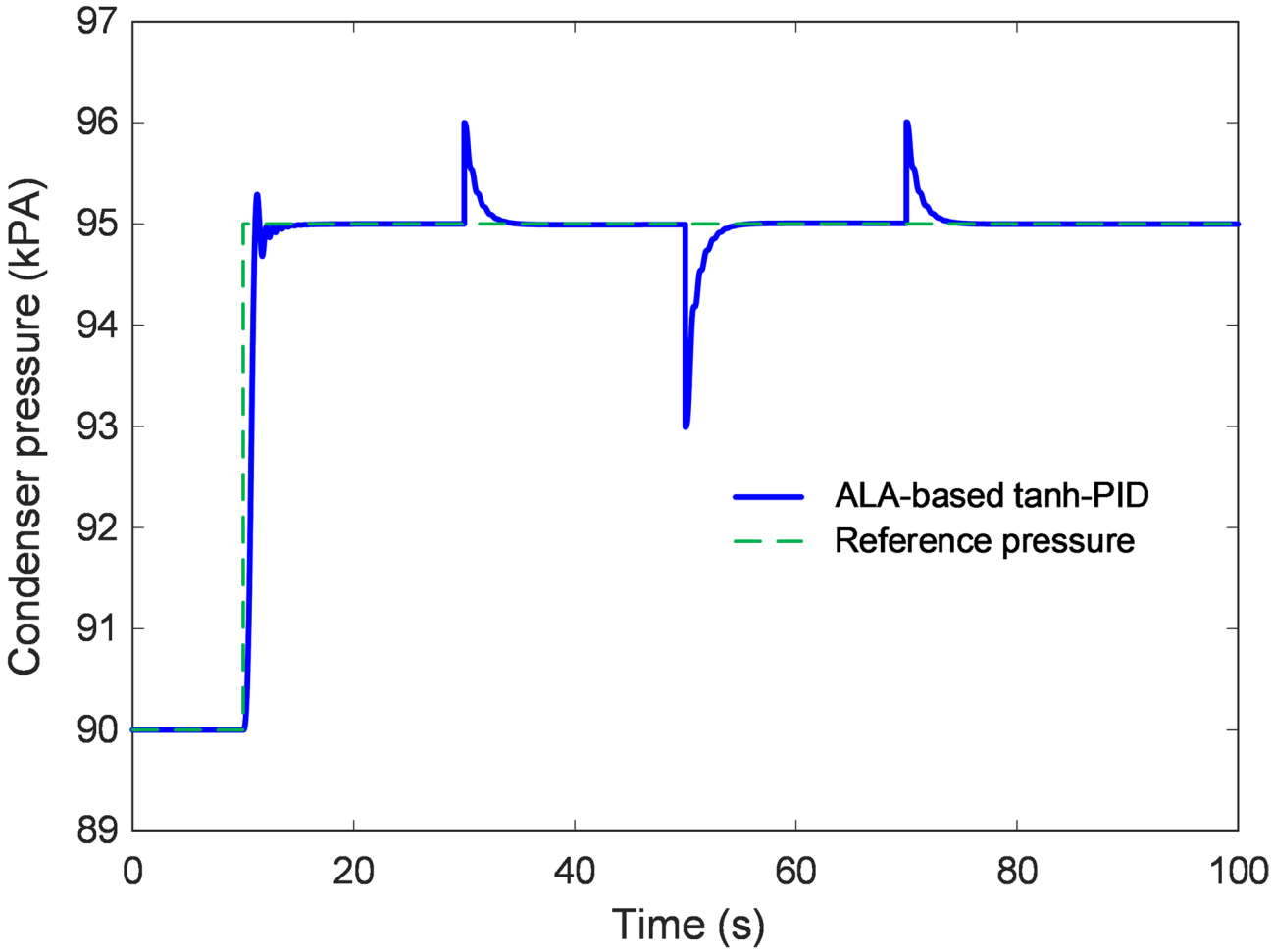


Fig. 13. External disturbance rejection capability of ALA-based tanh-PID controller.

Data availability

The datasets used and/or analysed during the current study available from the corresponding author on reasonable request.

Received: 31 August 2025; Accepted: 30 December 2025
Published online: 10 January 2026

References

1. Jabari, M. et al. Efficient pressure regulation in nonlinear shell-and-tube steam condensers via a Novel TDn(1 + PIDn) controller and DCSA algorithm. *Sci. Rep.* **15**, 2090 (2025).
2. Jabari, M., Izci, D., Ekinci, S., Bajaj, M. & Zaitsev, I. Performance analysis of DC-DC Buck converter with innovative multi-stage PIDn(1+PD) controller using GEO algorithm. *Sci. Rep.* **14**, 25612 (2024).
3. Åström, K. J. & Hägglund, T. The future of PID control. *Control. Eng. Pract.* **9**, 1163–1175 (2001).
4. Çelik, E. Exponential PID controller for effective load frequency regulation of electric power systems. *ISA Trans.* **153**, 364–383 (2024).
5. Hasan, M. W., Mohammed, A. S. & Noaman, S. F. An adaptive neuro-fuzzy with nonlinear PID controller design for electric vehicles. *IFAC J. Syst. Control* **27**, 100238 (2024).
6. Baihan, A. et al. A hybrid meta-heuristic algorithm for optimum micro-robotic position control with PID controller. *Int. J. Comput. Intell. Syst.* **18**, 86 (2025).
7. Eker, E., Izci, D., Ekinci, S., Elsayed, F. & Salman, M. A Novel 2-DOF PIDA control strategy with GCRA-based parameter optimization for electric furnace temperature control. *PLoS ONE* **20**, e0334594 (2025).
8. Tepljakov, A. et al. FOPID controllers and their industrial applications: A survey of recent results. *IFAC-PapersOnLine* **51**, 25–30 (2018).
9. Basil, N. et al. Performance analysis of hybrid optimization approach for UAV path planning control using FOPID-TID controller and HAOAROA algorithm. *Sci. Rep.* **15**, 4840 (2025).
10. Ansari, S., Chandel, A. & Tariq, M. A comprehensive review on power converters control and control strategies of AC/DC microgrid. *IEEE Access* **9**, 17998–18015 (2021).
11. Arya, Y. et al. Cascade-I λ D μ N controller design for AGC of thermal and hydro-thermal power systems integrated with renewable energy sources. *IET Renew. Power Gener.* **15**, 504–520 (2021).
12. El-Sousy, F. F. M. et al. New cascaded 1+PII2D/FOPID load frequency controller for modern power grids including superconducting magnetic energy storage and renewable energy. *Fract. Fract.* **7**, 672 (2023).

13. Izci, D. et al. A novel cascaded RPIDD2-PI controller tuned by enhanced cooperation search algorithm for automatic voltage regulator systems. *IET Control Theory Appl.* **19**, (2025).
14. Sahin, A. K., Cavdar, B. & Ayas, M. S. An adaptive fractional controller design for automatic voltage regulator system: Sigmoid-based fractional-order PID controller. *Neural. Comput. Appl.* **36**, 14409–14431 (2024).
15. Chetty, N. D., Sharma, G., Gandhi, R. & Çelik, E. A novel salp swarm optimization oriented 3-DOF-PIDA controller design for automatic voltage regulator system. *IEEE Access* **12**, 20181–20196 (2024).
16. Ekinci, S. et al. Optimizing AVR system performance via a novel cascaded RPIDD2-FOPI controller and QWGBO approach. *PLoS ONE* **19**, e0299009 (2024).
17. Khokhar, B., Dahiya, S. & Parmar, K. P. S. A novel hybrid fuzzy PD-TID controller for load frequency control of a standalone microgrid. *Arab J. Sci. Eng.* **46**, 1053–1065 (2021).
18. Gopi, P., Reddy, S. V., Bajaj, M., Zaitsev, I. & Prokop, L. Performance and robustness analysis of V-Tiger PID controller for automatic voltage regulator. *Sci. Rep.* **14**, 7867 (2024).
19. Ekinci, S. et al. Advanced control parameter optimization in DC motors and liquid level systems. *Sci. Rep.* **15**(1), 1394 (2025).
20. Turab, N. et al. Adaptive sliding mode control for chaotic system synchronization using neural networks. *Sci. Rep.* **15**(1), 37547 (2025).
21. Al Samman, F. M., Khaliq, W. A., Hilali, S. O., Niazi, A. U. K. & Smerat, A. Adaptive neural network based leader-following consensus control for a class of second-order nonlinear multi-agent systems: F. Al Samman et al.. *Sci. Rep.* **15**(1), 36040 (2025).
22. Gupta, M. et al. Grid-connected PV inverter system control optimization using Grey Wolf optimized PID controller. *Sci. Rep.* **15**(1), 28869 (2025).
23. Izci, D., Ekinci, S., Rizk-Allah, R. M., Alribdi, N. I., Smerat, A., Alzahrani, A., Alwadain, A., Snasel, V. & Abualigah, L. Master–slave architecture enhanced and Improved GBO tuned cascaded PI-PDN controller for speed regulation of DC motors. *Optimal Control Appl. Methods* (2025).
24. Jabari, M. et al. An advanced PID tuning method for temperature control in electric furnaces using the artificial Rabbits optimization algorithm. *Int. J. Dyn. Control* **13**(5), 1–15 (2025).
25. Hussein, A. M. et al. A hybrid PSO-GCRA framework for optimizing control systems performance. *Int. J. Robot. Control Syst.* **5**(1), 459–478 (2025).
26. Jan, F. U., Badar, R., Al-Shamayleh, A. S., Uehara, A., Senjyu, T. & Akhunzada, A. Soft computing based damping controllers with online parameters tuning for stability enhancement of power systems. *IEEE Access* (2025).
27. Izci, D. et al. Refined sinh cosh optimizer tuned controller design for enhanced stability of automatic voltage regulation. *Electr. Eng.* **106**(5), 6003–6016 (2024).
28. Izci, D., Abualigah, L., Can, Ö., Andiç, C. & Ekinci, S. Achieving improved stability for automatic voltage regulation with fractional-order PID plus double-derivative controller and mountain gazelle optimizer. *Int. J. Dyn. Control* **12**(7), 2550–2565 (2024).
29. Aribowo, W. et al. Controlling parameters proportional integral derivative of DC motor using a gradient-based optimizer. *Int. J. Power Electron. Drive Syst.* **15**(2), 696–703. https://doi.org/10.11591/ijpeds.v15.i2.pp696-703 (2024).
30. Abualigah, L., Ekinci, S. & Izci, D. Aircraft pitch control via filtered proportional-integralderivative controller design using sinh cosh optimizer. *Int. J. Robot. Control Syst.* **4**(2), 746–757 (2024).
31. Abualigah, L., Izci, D., Ekinci, S. & Zitar, R. Optimizing aircraft pitch control systems: A novel approach integrating artificial Rabbits optimizer with PID-F controller. *Int. J. Robot. Control Syst.* **4**(1), 354–364 (2024).
32. Tanabe, R. & Fukunaga, A. S. Improving the search performance of SHADE using linear population size reduction. In *2014 IEEE Congress on Evolutionary Computation (CEC)* 1658–1665 (IEEE, 2014). https://doi.org/10.1109/CEC.2014.6900380.
33. Chauhan, D. & Yadav, A. An adaptive artificial electric field algorithm for continuous optimization problems. *Expert Syst* **40**, e13380 (2023).
34. Dehghani, M., Montazeri, Z., Trojovská, E. & Trojovský, P. Coati optimization algorithm: A new bio-inspired metaheuristic algorithm for solving optimization problems. *Knowl. Based Syst.* **259**, 110011 (2023).
35. Zhao, S., Zhang, T., Ma, S. & Chen, M. Dandelion optimizer: A nature-inspired metaheuristic algorithm for engineering applications. *Eng. Appl. Artif. Intell.* **114**, 105075 (2022).
36. Li, S.-X. & Wang, J.-S. Dynamic modeling of steam condenser and design of PI controller based on grey wolf optimizer. *Math. Probl. Eng.* **2015**, 1–9 (2015).
37. Ekinci, S. et al. Optimizing steam condenser efficiency: Integrating logarithmic spiral search and greedy selection mechanisms in gazelle optimizer for PI controller tuning. *Result. Eng.* **24**, 103501 (2024).
38. Alzakari, S. A., Izci, D., Ekinci, S., Alhussan, A. A. & Hashim, F. A. Nonlinear FOPID controller design for pressure regulation of steam condenser via improved metaheuristic algorithm. *PLoS ONE* **19**, e0309211 (2024).
39. Ekinci, S. et al. Optimized FOPID controller for steam condenser system in power plants using the sinh-cosh optimizer. *Sci. Rep.* **15**, 6876 (2025).
40. Ekinci, S. et al. A novel pressure control method for nonlinear shell-and-tube steam condenser system via electric eel foraging optimizer. *Sci. Rep.* **15**, 7550 (2025).
41. Oravec, J. et al. Robust model predictive control and PID control of shell-and-tube heat exchangers. *Energy* **159**, 1–10 (2018).
42. Wu, T., Ge, Z., Yang, L. & Du, X. Transient behavior of the cold end system in an indirect dry cooling thermal power plant under varying operating conditions. *Energy* **181**, 1202–1212 (2019).
43. Ali, L. F., Al-Samarraie, S. A. & Humaidi, A. J. Performance of double pipe heat exchanger—partially occupied by metal foam—is better enhanced using robust adaptive barrier function-based sliding mode control. *Energies Basel* **18**, 4671 (2025).
44. Ali, L. F. & Humaidi, A. J. Offset temperature and amplitude-frequency effect on convection heat transfer in partially gradient porous cavity with different outlet port locations. *Processes* **13**, 2279 (2025).
45. Al-Dujaili, A. Q. et al. Maximizing solar energy utilization and controlling electrical consumption in domestic water heaters by integrating with aluminum reflector. *Measurement* **230**, 114558 (2024).
46. Xiao, Y., Cui, H., Khurma, R. A. & Castillo, P. A. Artificial lemming algorithm: A novel bionic meta-heuristic technique for solving real-world engineering optimization problems. *Artif. Intell. Rev.* **58**, 84 (2025).
47. Wang, J.-S. & Li, S.-X. PID controller of steam condenser based on particle swarm optimization algorithm. *J. Comput. Theor. Nanosci.* **14**, 3698–3701 (2017).
48. Izci, D. et al. A novel control scheme for automatic voltage regulator using novel modified artificial rabbits optimizer. *e-Prime Adv. Electr. Eng. Electron. Energy* **6**, 100325 (2023).
49. Ekinci, S., Izci, D., Can, O., Bajaj, M. & Blazek, V. Frequency regulation of PV-reheat thermal power system via a novel hybrid educational competition optimizer with pattern search and cascaded PDN-PI controller. *Results Eng.* **24**, 102958 (2024).

Author contributions

Serdar Ekinci, Davut Izci, Mostafa Jabari: Conceptualization, Methodology, Software, Visualization, Investigation, Writing—Original draft preparation, Mohit Bajaj: Data curation, Validation, Supervision, Resources, Writing—Review and Editing. Emre Çelik, Pradeep Vishnuram, Olena Rubanenko: Project administration, Supervision, Resources, Writing—Review and Editing.

Funding
This research received no specific grant from any funding agency in the public, commercial, or not-for-profit sectors.

Declarations

Competing interests
The authors declare no competing interests.

Additional information
Correspondence and requests for materials should be addressed to M.B. or O.R.

Reprints and permissions information is available at www.nature.com/reprints.

Publisher's note Springer Nature remains neutral with regard to jurisdictional claims in published maps and institutional affiliations.

Open Access This article is licensed under a Creative Commons Attribution-NonCommercial-NoDerivatives 4.0 International License, which permits any non-commercial use, sharing, distribution and reproduction in any medium or format, as long as you give appropriate credit to the original author(s) and the source, provide a link to the Creative Commons licence, and indicate if you modified the licensed material. You do not have permission under this licence to share adapted material derived from this article or parts of it. The images or other third party material in this article are included in the article's Creative Commons licence, unless indicated otherwise in a credit line to the material. If material is not included in the article's Creative Commons licence and your intended use is not permitted by statutory regulation or exceeds the permitted use, you will need to obtain permission directly from the copyright holder. To view a copy of this licence, visit http://creativecommons.org/licenses/by-nc-nd/4.0/.

© The Author(s) 2026, corrected publication 2026